Inorganic Chemistry
Article

Inorg. Chem. **2010**, *49*, 6013–6025 **6013**
DOI: 10.1021/ic100549u

Efficient Phosphodiester Hydrolysis by Luminescent Terbium(III) and Europium(III) Complexes

Maryene A. Camargo,[†] Ademir Neves,[*,†] Adailton J. Bortoluzzi,[†] Bruno Szpoganicz,[†] Franciele L. Fischer,[‡] Hernán Terenzi,[*,‡] Osvaldo A. Serra,[§] Vanessa G. Santos,[∥] Boniek G. Vaz,[∥] and Marcos N. Eberlin[∥]

[†]*Laboratório de Bioinorgânica e Crystalografia (LABINC), Departamento de Química, and* [‡]*Centro de Biologia Molecular Estrutural, Departamento de Bioquímica, CCB,* [§]*Laboratório de Terras Raras (FFCLRP-USP), Departamento de Química, Universidade de São Paulo, Avenue Bandeirantes 3900, 14040-901, Ribeirão Preto, São Paulo, Brazil,* [∥]*Laboratório ThoMSon de Espectrometria de Massas, Instituto de Química, Universidade Estadual de Campinas, 13083-970, Campinas, São Paulo, Brazil, and Universidade Federal de Santa Catarina, 88040-900 Florianópolis, Santa Catarina, Brazil*

Received March 23, 2010

The synthesis and structures of two new isostructural mononuclear $[Ln(L)(NO_3)(H_2O)_3](NO_3)_2$ complexes, with Ln = Tb (complex **1**) and Eu (complex **2**), which display high activity in the hydrolysis of the substrate 2,4-bis-(dinitrophenyl)phosphate, are reported. These complexes displayed catalytic behavior similar to the mononuclear gadolinium complex $[Gd(L)(NO_3)(H_2O)_3](NO_3)_2$ previously reported by us (*Inorg. Chem.* **2008**, *47*, 2919−2921); one hydrolysis reaction in two stages where the diesterase and monoesterase activities could be monitored separately, with the first stage dependent on and the second independent of the complex concentration. Through potentiometric studies, electrospray ionization mass spectrometry (ESI-MS) analysis, and determination of the kinetic behaviors of **1** and **2** in acetonitrile/water solution, the species present in solution could be identified and suggested a dinuclear species, with one hydroxo group, as the most prominent catalyst under mild conditions. The complexes show high activity (k_1 = 7 and 18 s^{-1} for **1** and **2**, respectively) and catalytic efficiency. Complexes **1** and **2** were found to be active toward the cleavage of plasmid DNA, and complete kinetic studies were carried out. Studies with a radical scavenger (dimethylsulfoxide) confirmed the hydrolytic action of **1** and **2** in the cleavage of DNA. Studies on the incubation of distamycin with plasmid DNA suggested that **1** and **2** are regio-specific, interacting with the minor groove of DNA. These complexes displayed luminescent properties. Complex **1** showed higher emission intensity than **2** due to a more efficient energy transfer between triplet and emission levels of terbium ($T \rightarrow {}^5D_4$), along with nonradiative deactivation mechanisms of the excited states of europium via multiphonon decays and the ligand-to-metal charge transfer state. Lifetime measurements of the $^5D_4$ and $^5D_0$ excited levels for **1** and **2**, respectively, indicated the numbers of coordinated water molecules for the complexes.

Introduction

The building blocks of nucleic acid polymers are linked through phosphodiester functional groups. Their remarkable stabilities make the hydrolytic cleavage of DNA particularly challenging, necessitating the use of enzyme catalysts (nucleases). As in the case of natural nucleases, a hydrolytic rather than oxidative cleavage mechanism is desirable since the oxidative cleavage produces diffusible free radicals, which is undesirable for molecular biology or clinical applications. For molecular biology applications, radical abstraction results in strand ends that cannot be enzymatically religated. For clinical applications, oxidative cleavage can cause indiscriminant peripheral damage to the cell, and radical diffusions may significantly hinder the specificity of cleavage that can be achieved. For these reasons, there is an open field for the development of lanthanide-based nucleases, which act as hydrolytic catalysts.[1]

The ability of the lanthanide ions to readily catalyze the hydrolysis of DNA is notable,[2] particularly in comparison to biologically relevant transition metals or alkaline earth Lewis acids, such as Zn, Ca, and Mg. This reflects the absence of redox chemistry and the high Lewis acidity associated with trivalent and tetravalent lanthanide ions. Also, these ions show fairly rapid ligand-exchange kinetics favorable from the viewpoint of reactant binding and product release. Consequently, the cleavage of the phosphodiester linkage of nucleic acids by lanthanide ions has been the subject of several recent studies.[3,4]

*Corresponding author. E-mail: ademir@qmc.ufsc.br.

(1) Shigekawa, H.; Ishida, M.; Miyake, K. *Appl. Phys. Lett.* **1999**, *74*, 460–463.
(2) Franklin, S. J. *Curr. Opin. Chem. Biol.* **2001**, *5*, 201–208.
(3) Rittich, B.; Spanová, A.; Falk, M.; Benes, M. J.; Hrubý, M. *J. Chromatogr., B: Anal. Technol. Biomed. Life Sci.* **2004**, *800*, 169–173.

Published on Web 06/04/2010

However, free ions of lanthanide are relatively weak catalysts due to the low solubility of the respective Ln-hydroxides in combination with the relatively high pK_a values of lanthanide aquo ions. Also, the lanthanide free ions are toxic to biological systems due to their similarity with Ca^{II} ions. Thus, the complexation of these ions is required. Many examples of lanthanide complexes with efficient catalytic behavior in the hydrolysis of phosphate diesters have been reported, such as lanthanide ions coordinated to amine phenolate multidentate ligands,[5] polyhydroxyl ligands (1,3-bis[tris(hydroxymethyl)methylamino]propane, BTP),[6] Schiff base macrocycles,[7] crown ethers and azacrowns,[8] amino acids,[9] etc.

The considerable cooperativity between lanthanide and hydroxo ions in the hydrolysis of phosphate esters is well-known.[10] Lanthanide ions complexed by BTP, for example, have shown significant catalytic activity in 2,4-bis-(dinitrophenyl)phosphate (BNPP) and *p*-nitrophenylphosphate (NPP) substrate hydrolysis,[11]due to the Ln-BTP system permiting a higher solubility of lanthanide ions (no hydroxide precipitation was observed in basic solutions) and to the cooperative effect of the hydroxide groups of the ligand acting as general bases.

The lanthanide systems show greater ability to form dimers and aggregates in solution, hindering these studies, especially in terms of defining the active catalytic species in the medium. However, through luminescence studies, it is possible to monitor the active metal site in catalysis, determining the active species involved in the kinetics.[12] Lanthanide ions are species with unique luminescence properties, characteristic narrow-line emission and long luminescence lifetimes in the order of milliseconds.[13]

Most metal ions essential or important for biological and functional structures show no luminescence in biological environments. However, the trivalent europium (Eu^{III}) and terbium (Tb^{III}) ions can keep their luminescent characteristics when they are artificially incorporated in biological systems.[14] Furthermore, the sensitivity of the excitation and emission spectra of Eu^{III} and Tb^{III} ions for specific structural factors, associated with the relatively high intensities of their spectral emission lines (under various sample conditions), indicates the potential of the Eu^{III} and Tb^{III} ions as candidates for ideal luminescent probes in biomolecular systems,[15] such as in deoxyribonucleic acid (DNA) or ribonucleic acid (RNA).[16,17]

In a recent publication,[18] we reported the $[Gd(H_2L)(NO_3)(H_2O)_3](NO_3)_2$ complex with a high efficiency toward the hydrolysis of the activated substrate 2,4-bis(dinitrophenyl)phosphate (BDNPP) and the cleavage of plasmid DNA. Solution studies indicate a dinuclear species as the most prominent catalyst under mild conditions. Stimulated by the promising results obtained in these studies, we report herein the synthesis and the structure of two new isostructural mononuclear $[Ln(L)(NO_3)(H_2O)_3](NO_3)_2$ complexes, with Ln = Tb (**1**) or Eu (**2**), which also displays high efficiency toward the hydrolysis of the substrate BDNPP. The respective active catalytic species were proposed through potentiometric studies and electrospray ionization mass spectrometry (ESI-MS) analysis of **1** and **2**, and through their kinetic behaviors in acetonitrile/water solution. Complexes **1** and **2** were found to be active toward the cleavage of plasmid DNA, and complete kinetic studies were carried out. Studies with a specific quencher of hydroxyl radicals and a DNA minor groove binding molecule (dimethylsulfoxide (DMSO) and distamycin, respectively) demonstrated a hydrolytic mechanism of action for **1** and **2** in terms of the plasmid DNA cleavage and regio-specificity, to the minor groove of DNA. These complexes display luminescent properties, which could be explored, and consequently, additional information regarding the active catalytic species was obtained.

Experimental Section

Materials and Measurements. 2-bis-[{(2-Pyridyl-methyl)aminomethyl}-6-{(2-hydroxy-benzyl)-(2-pyridyl-methyl)}aminomethyl]-4-methyl-phenol (H_2L) and BDNPP were synthesized by previously described methods.[19,20] All other chemicals and solvents were of analytical or spectroscopic grade purchased from commercial sources and used without further purification. Infrared spectra were recorded on a Perkin-Elmer model 16PC spectrometer, in KBr pellets in the 4000−400 cm^{-1} range. Elemental analysis was performed on a Carlo Erba E-1110 instrument. The mass spectrometry (MS) experiments were carried out using a Q-TOF mass spectrometer (Micromass, Manchester, UK) and electrospray ionization in the positive mode (ESI(+)-MS). Typical MS conditions were: source temperature of 100 °C, desolvation temperature of 100 °C, capillary voltage of 3 kV, and cone voltage of 50 V. The sample was injected using a syringe pump (Harvard Apparatus) at a flow rate of 5 μL/min. Mass spectra were acquired in the range of 50−2000 m/z. The luminescence properties at room and liquid nitrogen temperatures were evaluated using a Jobin-Yvon FLUOROLOG3 spectrofluorometer; lifetime measurements and time-resolved spectra were performed using the same spectrofluorometer equipped with a phosphorimeter accessory 1934 D.

Synthesis of Complexes. **$[Tb(H_2L)(NO_3)(H_2O)_3](NO_3)_2$ (1).** Complex **1** was synthesized in methanolic solution by mixing the H_2L ligand (1.09 g, 2 mmol, 30 mL) and $Tb(NO_3)_3 \cdot 6H_2O$ (0.91 g, 2 mmol, 10 mL), with stirring and mild heating (40 °C) for 45 min. The solid obtained after total evaporation of the solvent was recrystallized in acetonitrile/acetone solution, yielding colorless monocrystals suitable for X-ray analysis. Yield: 79% (1.49 g,

(4) Kuzuya, A.; Machida, K.; Sasayama, T.; Shi, Y.; Mizoguchi, R.; Komiyama, M. *J. Alloys Compd.* **2006**, *408*−*412*, 396–399.
(5) Camargo, M. A.; Neves, A.; Szpoganicz, B.; Bortoluzzi, A. J.; Fischer, F. L.; Terenzi, H.; Castellano, E. E. *Inorg. Chem.* **2010**, *49*, 3057–3063.
(6) Gomez-Tagle, P.; Yatsimirsky, A. K. *Inorg. Chem.* **2001**, *40*, 3786–3796.
(7) Zhu, B.; Zhao, D.; Ni, J.; Ying, D.; Huang, B; Wang, Z. *J. Mol. Catal. A: Chem.* **1998**, *135*, 107–110.
(8) Chang, C. A.; Wu, B. H.; Kuan, B. Y. *Inorg. Chem.* **2005**, *44*, 6646–6654.
(9) Torres, J.; Brusoni, M.; Peluffo, F.; Kremer, C.; Domínguez, S.; Mederos, A.; Kremer, E. *Inorg. Chim. Acta* **2005**, *358*, 3320–3328.
(10) Calderón, A.; Yatsimirsky, A. K. *Inorg. Chim. Acta* **2004**, *357*, 3483–3492.
(11) Gómez-Tagle, P.; Yatsimirsky, A. K. *J. Chem. Soc., Dalton Trans.* **1998**, 2957–2959.
(12) Geyer, C. R.; Sem, D. *J. Mol. Biol.* **1998**, *275*, 483–489.
(13) Bunzli, J. G. *Acc. Chem. Res.* **2006**, *39*, 53–61.
(14) Cronce, D. T.; Horrocks, W. D., Jr. *Biochemistry* **1992**, *31*, 7963.
(15) Kitamura, Y.; Ihara, T.; Tsujimura, Y.; Osawa, Y.; Tazaki, M.; Jyo, A. *Anal. Biochem.* **2006**, *359*, 259–261.
(16) Yang, Z.-Y.; Wang, Y.; Wang, Y. *Bioorg. Med. Chem. Lett.* **2007**, *17*, 2096–2101.
(17) Li, S.; Yuan, W.; Zhu, C.; Xu, J. *Anal. Biochem.* **2004**, *331*, 235–242.
(18) Camargo, M. A.; Neves, A.; Bortoluzzi, A. J.; Szpoganicz, B.; Martendal, A.; Murgu, M.; Fischer, F. L.; Terenzi, H.; Severino, P. C. *Inorg. Chem.* **2008**, *47*, 2919–2921.
(19) Mitic, N.; Smith, S. J.; Neves, A.; Guddat, L. W.; Gahan, L. R.; Schenk, G. *Chem. Rev.* **2006**, *106*, 3338–3363.
(20) Bunton, C. A.; Farber, S. J. *J. Org. Chem.* **1969**, *34*, 767–772.

Table 1. Crystal Data and Structure Refinement of Complexes **1** and **2**

complex	**1**	**2**
empirical formula	$C_{34}H_{41}N_8O_{14}Tb$	$C_{34}H_{41}EuN_8O_{14}$
FW	944.67	937.71
temperature (K)	293(2) K	
$\lambda_{Mo\ K_\alpha}$ (Å)	0.71069	
crystal system	monoclinic	monoclinic
space group	$P2_1/n$	$P2_1/n$
unit cell dimensions		
a (Å)	19.231(4)	19.301(3)
b (Å)	10.270(3)	10.302(2)
c (Å)	19.6270(10)	19.700(2)
β (°)	102.76(2)	102.82(1)
V (Å^3)	3780.6(14)	3819.5(10)
Z	4	4
D_{calc} (Mg/m^3)	1.658	1.631
μ (mm^{-1})	1.950	1.720
$F(000)$	1912	1904
crystal size (mm^3)	0.26 × 0.16 × 0.10	0.33 × 0.20 × 0.13
θ range (°)	1.34−25.09	1.34−25.06
reflections collected	6935	6988
independent reflections	6725 (R_{int} = 0.0375)	6776 (R_{int} = 0.0358)
absorption correction	ψ-scan	
max. and min. transmission	0.8200 and 0.7128	0.7958 and 0.6842
refinement method	full-matrix least squares on F^2	
data/restraints	6725/93	6776/96
parameters	549	552
goodness-of-fit (F^2)	1.054	1.054
final R indices [$I > 2\sigma(I)$]	R_1 = 0.0361, wR_2 = 0.0846	R_1 = 0.0328, wR_2 = 0.0775
R indices (all data)	R_1 = 0.0635, wR_2 = 0.0929	R_1 = 0.0518, wR_2 = 0.0828

1.58 mmol). IR, cm^{-1} (KBr pellet): 3566−2840 (ν C−H$_{ar}$, C−H$_{alif}$, O−H); 1608−1430 (ν C=C, C=N); 1470, 1384, 1312 (ν NO_3^-); 1264 (ν CO_{phenol}); 758 (δ C−H$_{ar}$). Anal. calcd for $TbC_{34}H_{41}N_8O_{14}$: C, 43.23; H, 4.37; N, 11.86%. Found: C, 43.32; H, 4.48; N, 11.93%.

[Eu(H$_2$L)(NO$_3$)(H$_2$O)$_3$](NO$_3$)$_2$ (2). Complex **2** was synthesized by the method previously described for complex **1** with the use of $Eu(NO_3)_3 \cdot 6H_2O$ instead of $Tb(NO_3)_3 \cdot 6H_2O$, yielding red monocrystals suitable for X-ray crystallographic analysis. Yield: 81%. IR, cm^{-1} (KBr pellet): 3566−2840 (ν C−H$_{ar}$, C−H$_{alif}$, O−H); 1608−1430 (ν C=C, C=N); 1470, 1384, 1312 (ν NO_3^-); 1264 (ν CO_{phenol}); 758 (δ C−H$_{ar}$). Anal. calcd for $EuC_{34}H_{41}N_8O_{14}$: C, 43.55; H, 4.41; N, 11.95%. Found: C, 43.42; H, 4.47; N, 11.84%.

Note: Attempts were made to synthesize dinuclear complexes, starting from a 2:1 stoichiometry ($Ln(NO_3)_3$:H_2L), however, only mononuclear compounds of the type $[Ln(H_2L)(NO_3)(H_2O)_3](NO_3)_2$ with Ln = Tb (**1**) and Eu (**2**) were obtained in solid state (monocrystals). Thus, the dinuclear complexes observed and detected in solution (ESI analysis and potentiometric titrations) could not be isolated.

Single-Crystal X-ray Structure Determination. For both complexes, the intensity data were collected with an Enraf-Nonius CAD4 diffractometer, at room temperature, with graphite-monochromated Mo K$_\alpha$ radiation. Cell parameters were determined from 25 centered reflections using a standard procedure.[21] All data were corrected for Lorentz and polarization effects.[22] A semiempirical absorption correction based on the azimuthal scans of seven appropriate reflections was also applied to the collected intensities with the PLATON program.[23,24] The structure was solved by direct methods and refined by full-matrix least squares methods using SIR97[25] and SHELXL97[26] programs, respectively. All nonhydrogen atoms were refined anisotropically. Hydrogen (H) atoms attached to carbon (C) atoms were placed at their idealized positions, with C−H distances and U_{eq} values taken from the default settings of the refinement program. H atoms of the water molecules and the amine group were found from Fourier difference map and treated with riding model. Uncoordinated phenol shows rotational disorder, where oxygen atom is partially bonded to C53 and C56 carbon atoms with site occupancies in complex **1** of 0.521(11) and 0.479(11) and in complex **2** of 0.525(9) and 0.475(9) for O50 and O50′, respectively. In complex **1**, the H atom of the phenol group could not be located. One uncoordinated nitrate anion also shows rotational disorder, and its oxygen atoms occupy two alternative positions with refined occupation factors of 0.750(12) and 0.250(12) in complex **1** and 0.562(17) and 0.438(17) in complex **2**. Further crystallographic information are given in Table 1.

Potentiometric Titrations. The potentiometric studies were carried out with a Corning-350 research pH meter fitted with blue-glass and Ag/AgCl reference electrodes calibrated to read −log [H$^+$] directly. The electrode was calibrated using the data obtained from a potentiometric titration of a known volume of a standard 0.10 mol L^{-1} HCl solution with a standard 0.10 mol L^{-1} KOH solution. The ionic strength of the HCl solution was maintained at 0.10 mol L^{-1} by addition of KCl. Measurements were carried out in a thermostatted cell containing a solution of the complex (0.05 mol/50 mL) with ionic strength adjusted to 0.10 mol L^{-1} by addition of KCl at 25.00 ± 0.05 °C. The experiments were performed under argon to eliminate the presence of atmospheric CO_2. All of the experimental solutions were prepared in acetonitrile/water (1:1, v/v), owing to the low solubility of the complexes in water. The pK_w of the acetonitrile/water containing 0.10 mol L^{-1} of KCl was 15.40.[27] Computations were carried out with the BEST7 program, and species diagrams were obtained with SPE and SPEPLOT programs.[28]

(21) *CAD-4 EXPRESS*, version 5.1/1.2; Enraf-Nonius: Delft, The Netherlands, **1994**.
(22) Spek, A. L.*HELENA; CAD-4 Data Reduction Program*; University of Utrecht: Utrecht, The Netherlands, **1996**.
(23) Spek, A. L. *Acta Crystallogr*. **2009**, *D65*, 148–155.
(24) North, A. C. T.; Phillips, D. C.; Mathews, F. S. *Acta Crystallogr*. **1968**, *A24*, 351–359.
(25) Altomare, A.; Burla, M. C.; Camalli, M.; Cascarano, G.; Giacovazzo, C.; Guagliardi, A.; Moliterni, A. G. G.; Polidori, G.; Spagna, R. *J. Appl. Crystallogr*. **1999**, *32*, 115–119.
(26) Sheldrick, G. M. *Acta Crystallogr*. **2008**, *A64*, 112–122.
(27) Herrador, M. A.; González, A. G. *Talanta* **2002**, *56*, 769–775.
(28) Martell, A. E.; Motekaitis, R. J. *Determination and Use of Stability Constants*; 2nd ed.; VCH: New York, 1992.

Reactivity. Kinetic experiments for the hydrolysis of the model substrate BDNPP were monitored spectrophotometrically for the absorbance increase at 400 nm due to the formation of 2,4-dinitrophenolate over time, under conditions of excess complex at 25 °C, and the reaction mixtures were monitored until saturation was reached. In these experiments, all of the mixture solutions were in an acetonitrile/water (3:1 v/v) medium. The systems showed high catalytic activity, and this could only be studied through the stopped-flow technique. The stopped-flow apparatus (model SX-18MV) and the associated computer system were manufactured by Applied Photophysics. The data were analyzed with the SX-18MV operating software. A total of 150 μL per sample was placed in a 1 cm thermostatically controlled cell compartment. The experiments were carried out in triplicate. The pseudofirst-order rate constants k_{obs} (s^{-1}) were calculated from the first-order exponential decay plot of absorbance versus time. Studies on the effects of pH on the hydrolysis reaction were performed in the pH range of 3.5−10.0 (MES pH 3.5−6.5; HEPES pH 7.0−8.0; CHES pH 9.0−10.0; I = 0.1 mol·L^{-1} with $LiClO_4$), under a 50-fold excess of complex, at 25 °C. Experiments to determine the dependence of the reaction rate on the complex concentration (5×10^{-4} to 5×10^{-3} mol L^{-1}) were carried out at 25 °C, pH of 7.0, with the BDNPP substrate (4×10^{-5} mol L^{-1}). In order to establish the number of molecules of substrate which are hydrolyzed per molecule of complex, the reaction was monitored at 445 nm, under a 50-fold substrate excess at pH of 7.0 and 25 °C. Isotopic effects of deuterium on the hydrolysis of BDNPP promoted by complexes **1** and **2** were investigated monitoring parallel reactions, where the buffer HEPES solutions at pH of 7.0 and pD of 7.0 were prepared in H_2O and D_2O, respectively.

DNA cleavage. Plasmid DNA cleavage experiments were carried out at different concentrations of complexes **1** and **2** with 500 ng (40 μM DNA base pairs (bp)) of pBSK-II plasmid DNA, in a final volume of 20 μL. Samples were incubated for 6 h at 50 °C with 25 mM PIPES at pH of 6.1, 6.5, 7.0, and 7.5, and 25% acetonitrile (v/v), with different final complex concentrations between 0 and 160 μM. After determination of the best conditions for the assay, kinetics experiments were performed, and time- and concentration-dependent cleavages were observed. Supercoiled plasmid DNA (510 ng) was incubated at 50 °C with **1** and **2** at several concentrations in PIPES buffer at pH of 7.0. At fixed time intervals up to 120 min for **1** and 360 min for **2**, samples were collected and analyzed by gel electrophoresis. To study the mechanism of the DNA cleavage reaction performed by complexes **1** and **2**, 10% DMSO was added to the reaction mixtures prior to addition of the complexes. Samples were incubated for 6 h at 50 °C and pH of 7.0. For the distamycin competition assays, DNA was preincubated in the presence of 50 μM distamycin for 30 min and then incubated for 6 h with the complex at 50 °C and 25 mM PIPES buffer at pH of 7.0. For all tests, samples were submitted to agarose gel electrophoresis and stained with ethidium bromide. The resulting gels were digitized with a photo documentation system (UVP Inc., Upland, CA), and DNA bands were quantified using LabWorks software version 4.0 (UVP).

Results and Discussion

X-ray Structural Characterization. Crystal structures of the complexes $[Tb(H_2L)(NO_3)(H_2O)_3](NO_3)_2$ (**1**) and $[Eu(H_2L)(NO_3)(H_2O)_3](NO_3)_2$ (**2**) were determined, and their ORTEP plots are shown in Figure 1. Selected bond lengths and angles are listed in Table 2.

Complexes **1** (colorless crystals) and **2** (red crystals) are isostructural consisting of a cation complex $[Ln(H_2L)(NO_3)(H_2O)_3]^{2+}$ and two nitrate anions as the counterion. Both complexes crystallize in the monoclinic crystal system and belong to $P2_1/n$ space group.

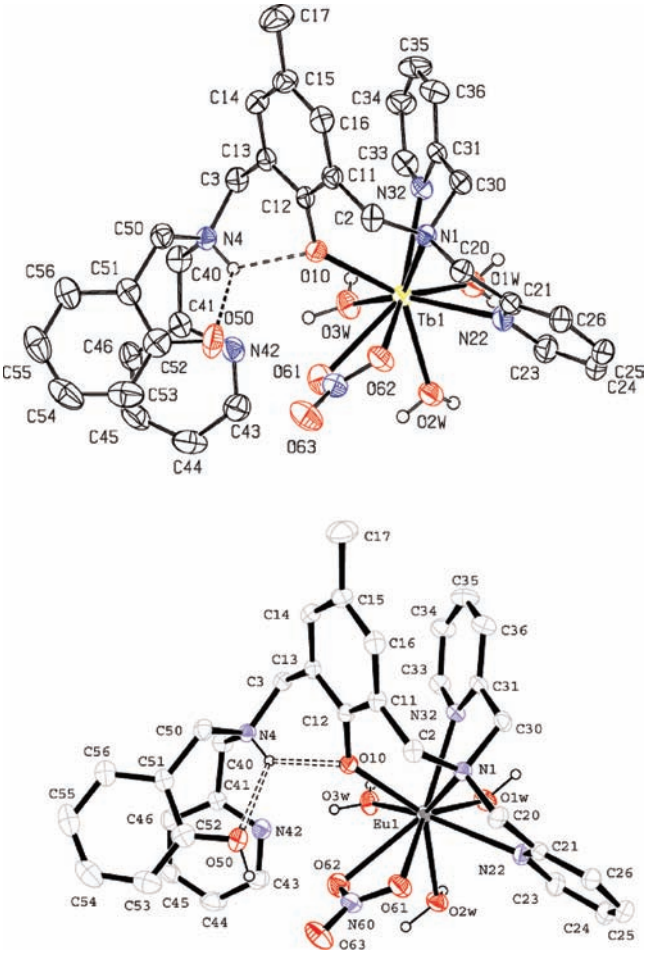

Figure 1. ORTEP plot diagrams of the cation complexes $[Tb(H_2L)(NO_3)(H_2O)_3]^{2+}$ (top) and $[Eu(H_2L)(NO_3)(H_2O)_3]^{2+}$(bottom).

Despite the unsymmetrical ligand H_2L containing two potentially distinct coordination moieties, which facilitates the generation of homo- and heterodinuclear mixed valence $M^{III}M^{II}$ complexes,[29−33] we present the formation of the mononuclear complexes, in which the Ln metal engages the available chelate on the soft side of the ligand, that is, one tertiary amine nitrogen atom N1, two pyridine nitrogen atoms N22 and N32, and one phenolate oxygen O10. The coordination sphere of each metal (CN = 9) is completed by three water molecules and one bidentate nitrate anion.

It is interesting to note that, in both of the structures of complexes **1** and **2**, the tertiary amine nitrogen atom N4, a component group of the hard site of the H_2L ligand, is protonated, which could be evidenced by the intramolecular

(29) Smith, S. J.; Casellato, A.; Hadler, K. S.; Mitic, N.; Riley, M. J.; Bortoluzzi, A. J.; Szpoganicz, B.; Schenk, G.; Neves, A.; Gahan, L. R. *J. Biol. Inorg. Chem.* **2007**, *12*, 1207–1220.
(30) Lanznaster, M.; Neves, A.; Bortoluzzi, A. J.; Aires, V. V. E.; Szpoganicz, B.; Terenzi, H.; Severino, P. C.; Fuller, J. M.; Drew, S. C.; Gahan, L. R.; Hanson, G. R.; Riley, M. J.; Schenk, G. *J. Biol. Inorg. Chem.* **2005**, *10*, 319–332.
(31) Lanznaster, M.; Neves, A.; Bortoluzzi, A. J.; Szpoganicz, B.; Schwingel, E. *Inorg. Chem.* **2002**, *41*, 5641–5643.
(32) Karsten, P.; Neves, A.; Bortoluzzi, A. J.; Lanznaster, M.; Drago, V. *Inorg. Chem.* **2002**, *41*, 4621–4626.
(33) Batista, S. C.; Neves, A.; Bortoluzzi, A. J.; Vencato, I.; Peralta, R. A.; Szpoganicz, B.; Aires, V. V. E.; Terenzi, H.; Severino, P. C. *Inorg. Chem. Commun.* **2003**, *6*, 1161–1165.

Table 2. Selected Bond Distances (Å) and Angles (°) for Complexes **1** and **2**

Complex 1			
Tb1−O10	2.263(3)	Tb1−N32	2.517(4)
Tb1−O1W	2.392(3)	Tb1−N22	2.605(4)
Tb1−O3W	2.397(4)	Tb1−N1	2.621(4)
Tb1−O2W	2.459(4)	Tb1−O61	2.666(4)
Tb1−O62	2.472(4)		
O10−Tb1−O1W	133.85(13)	O2W−Tb1−N22	75.30(13)
O10−Tb1−O3W	78.07(12)	O62−Tb1−N22	73.41(13)
O1W−Tb1−O3W	73.47(13)	N32−Tb1−N22	96.26(13)
O10−Tb1−O2W	135.38(12)	O10−Tb1−N1	75.71(12)
O1W−Tb1−O2W	70.94(13)	O1W−Tb1−N1	114.66(13)
O3W−Tb1−O2W	76.58(13)	O3W−Tb1−N1	149.00(12)
O10−Tb1−O62	84.29(13)	O2W−Tb1−N1	134.31(12)
O1W−Tb1−O62	141.77(13)	O62−Tb1−N1	71.50(12)
O3W−Tb1−O62	121.93(13)	N32−Tb1−N1	66.65(12)
O2W−Tb1−O62	78.89(13)	N22−Tb1−N1	63.46(13)
O10−Tb1−N32	76.01(13)	O10−Tb1−O61	71.83(12)
O1W−Tb1−N32	69.17(13)	O1W−Tb1−O61	129.95(13)
O3W−Tb1−N32	91.21(13)	O3W−Tb1−O61	72.97(13)
O2W−Tb1−N32	140.10(13)	O2W−Tb1−O61	65.92(12)
O62−Tb1−N32	136.88(13)	O62−Tb1−O61	48.98(13)
O10−Tb1−N22	137.77(13)	N32−Tb1−O61	146.38(13)
O1W−Tb1−N22	76.59(14)	N22−Tb1−O61	114.08(13)
O3W−Tb1−N22	144.12(13)	N1−Tb1−O61	113.33(13)
Complex 2			
Eu1−O10	2.290(3)	Eu1−N32	2.553(3)
Eu1−O1W	2.429(3)	Eu1−N22	2.631(4)
Eu1−O3W	2.430(3)	Eu1−N1	2.653(3)
Eu1−O2W	2.499(3)	Eu1−O61	2.508(3)
Eu1−O62	2.670(3)		
O10−Eu1−O1W	134.08(11)	O2W−Eu1−N22	75.40(11)
O10−Eu1−O3W	78.25(11)	O62−Eu1−N22	113.97(11)
O1W−Eu1−O3W	73.78(11)	N32−Eu1−N22	95.58(11)
O10−Eu1−O2W	136.09(10)	O10−Eu1−N1	75.50(10)
O1W−Eu1−O2W	70.76(11)	O1W−Eu1−N1	113.87(11)
O3W−Eu1−O2W	77.07(11)	O3W−Eu1−N1	148.59(10)
O10−Eu1−O62	72.06(10)	O2W−Eu1−N1	134.30 (10)
O1W−Eu1−O62	130.66(11)	O62−Eu1−N1	113.29(10)
O3W−Eu1−O62	73.77(11)	N32−Eu1−N1	65.96(11)
O2W−Eu1−O62	66.45(10)	N22−Eu1−N1	63.03(11)
O10−Eu1−N32	75.99(10)	O10−Eu1−O61	84.19(11)
O1W−Eu1−N32	69.05(11)	O1W−Eu1−O61	141.70(11)
O3W−Eu1−N32	91.21(11)	O3W−Eu1−O61	122.67(11)
O2W−Eu1−N32	139.81(11)	O2W−Eu1−O61	79.43(11)
O62−Eu1−N32	146.78(11)	O62−Eu1−O61	48.90(11)
O10−Eu1−N22	137.13(11)	N32−Eu1−O61	136.20(11)
O1W−Eu1−N22	76.33(12)	N22−Eu1−O61	73.24(11)
O3W−Eu1−N22	144.54(11)	N1−Eu1−O61	71.44(10)

hydrogen bonds (N4−H4···O10 and N4−H4···O50; Table 3) and by the bond lengths Tb−O10 or Eu−O10, typical of Ln−phenolate bonds.[34,35]

In complexes **1** and **2**, the Ln−$O_{phenolate}$ and Ln−N distances have average values of 2.280 and 2.597 Å, respectively. These distances are considerably larger than the average Fe−$O_{phenolate}$ (1.997 Å) and Fe−N (2.182 Å) distances found in the $[Fe^{II}Fe^{III}(bpmp)(bpc)_2](ClO_4)_2$ complex, where bpmp is 2,6-bis[(bis(2-pyridylmethyl)-amino)methyl]-4-methylphenolate and bpc is 4-biphenylcarboxylate.[36] However, the Ln−$O_{phenolate}$ and Ln−N distances in **1** and **2** are consistent with the bond lengths

Table 3. Hydrogen Bonds for Complexes **1** and **2** (Å and °)

	d(N−H)	*d*(H···O)	*d*(N···O)	<(NHO)
Complex 1				
N4−H4···O10	0.93	2.20	2.802(5)	122
N4−H4···O50	0.93	2.38	2.963(9)	121
Complex 2				
N4−H4···O10	0.88	2.15	2.809(4)	131
N4−H4···O50	0.88	2.41	2.954(8)	120

found in other terbium or europium complexes with aminophenolate ligands.[37,38]

The $[Gd(H_2L)(NO_3)(H_2O)_3](NO_3)_2$ complex, which we reported in previous studies,[18] is isostructural to complexes **1** and **2**, with slight differences in the Ln−O and Ln−N bond lengths within the series of three complexes. However, the bond lengths increase in the same order as the ionic radius of these metals (Eu > Gd > Tb). The bond angles of **1**, **2**, and the Gd complex are very similar, indicating that the H_2L ligand does not undergo an important deformation in its structure when coordinated with the metal ions Tb^{III}, Eu^{III}, or Gd^{III}.

Mass spectrometry. Complexes **1** and **2** were dissolved in an acetonitrile/water solution (75:25) at pH of 7 and analyzed by ESI-MS in the positive mode. The spectra (Figures S1 and S2 in the Supporting Information) showed a very similar solution composition for the two complexes. The ions "fished" by ESI[39,40] from **1,** such as those at *m*/*z* 702 (**1a**), 765 (**1b**), and 828 (**1c**), were also observed in their isostructural form for **2** at: *m*/*z* 696 (**2a**), 759 (**2b**), and 822 (**2c**). The dimers of the H_2L bond to Tb^{III} or Eu^{III} were found for almost every ion previously cited, and they are $\mathbf{1a}_d$, $\mathbf{1b}_d$ and $\mathbf{1c}_d$ for complex **1** and $\mathbf{2a}_d$, $\mathbf{2b}_d$ and $\mathbf{2c}_d$ for complex **2** (Figures S1 and S2 in the Supporting Information).

The X-ray crystal structure showed mononuclear complexes **1** and **2** in which Tb^{III} or Eu^{III} are bound to the soft side of the ligand. This binding is also observed in the ESI-MS via the ions detected at *m*/*z* 765 (**1b**) for **1** and 759 (**2b**) for **2.** The ions at *m*/*z* 702 (**1a**) and 828 (**1c**) for **1** and 696 (**2a**) and 822 (**2c**) for **2** correspond to mononuclear lanthanide complexes in which Tb^{III} and Eu^{III} ions reside at the hard side of the ligand (Figure 2). It is believed that in an acetonitrile/water solution, the lanthanide ion might flip to the hard site of the ligand with deprotonation of the second phenolate. This finding is in agreement with the higher affinity of lanthanide ions (Lewis acids) for hard bases.

In a recent publication,[18] we showed the same behavior for the isostructural gadolinium (Gd) complex, in which it is also proposed that this mononuclear species disproportionates forming a dinuclear Gd species and free ligand in solution. This process is also assumed for **1** and **2** with their ESI(+)-MS ions detected at *m*/*z* 546, which corresponds to the protonated free ligand and the dinuclear ions at *m*/*z* 1002 for **1d,** 1047 for **1e,** 988 for **2d**, and 1033 for **2e** (Figure 3). This finding is in agreement with the strong tendency of the lanthanide ions to form dinuclear complexes in solution.[41] As in the case of the mononuclear

(34) Lawrence, R. G.; Jones, C. J.; Kresinski, R. A. *J. Chem. Soc., Dalton Trans.* **1996**, 501–507.
(35) Paluch, M.; Lisowski, J. *J. Alloys Compd.* **2008**, *451*, 443–447.
(36) Maeda, Y.; Ishida, A.; Ohba, M.; Sugihara, S.; Hayami, S. *Bull. Chem. Soc. Jpn.* **2002**, *75*, 2441–2448.
(37) Paluch, M.; Lisowski, J. *J. Alloys Compd.* **2008**, *451*, 443–447.
(38) Wietzke, R.; Mazzanti, M.; Latour, J.; Pécaut, J.; Cordier, P.; Madic, C. *Inorg. Chem.* **1998**, *37*, 6690–6697.
(39) Sabino, A. A.; Machado, A. H. L.; Correia, C. R. D.; Eberlin, M. N. *Angew. Chem., Int. Ed.* **2004**, *43*, 2514–2518.
(40) Orth, E. S.; da Silva, P. L. F.; Mello, R. S.; Bunton, C. A.; Fiedler, H. D.; Milagre, H. M. S.; Eberlin, M. N.; Nome, F. *J. Org. Chem.* **2009**, *74*, 5011–5016.
(41) Farquhar, E. R.; Richard, J. P.; Morrow, J. R. *Inorg. Chem.* **2007**, *46*, 7169–7177.

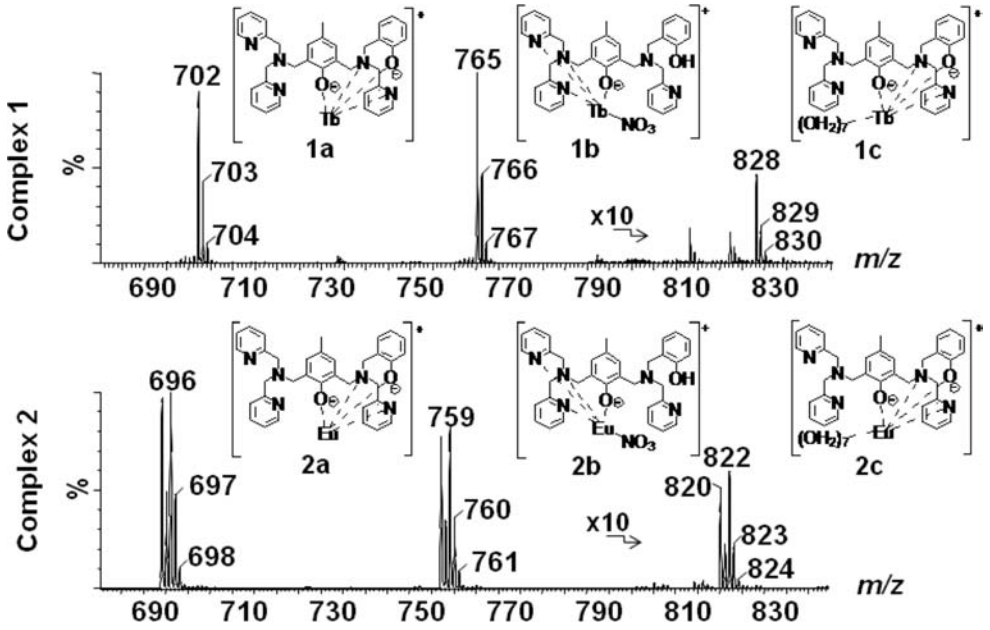

Figure 2. ESI(+)-MS of **1** and **2** "fished" from acetonitrile/water (75:25) solutions of these complexes.

complex, we also observed dimers of the ligand bound to dinuclear complex species (Figures S1 and S2 in the Supporting Information), such as $\mathbf{1d}_d$, $\mathbf{1e}_d$, and $\mathbf{2e}_d$.

Potentiometric Equilibrium Determinations. Although the titration studies were carried out through the dissolution of the corresponding complexes **1** and **2**, in an acidic environment (pH $\sim$ 2.5), it is believed that these complexes dissociate into the free ligand and the aqueous metal ion. Thus, it was necessary, first, to find the hydrolysis constants of the lanthanide ions[42] and to calculate the ligand protonation constants (Table 4).

Considering the principles of coordination chemistry, associated with the ESI-MS data of **1** and **2**, the equilibria 1−5 could be obtained. As complexes **1** and **2** showed similar behavior in solution, we used a common nomenclature for them (Ln).

Figure 4 shows the potentiometric titration curves for 0.05 mmol of complexes **1** and **2** solutions. Each curve gives information on the stoichiometry and the stability of possible species formed in solution. The curves for **1** and **2** have similar profiles, with four inflections giving a total "*a*" value of 6, showing that the addition of 6 mol of KOH per mole of metal ion is required to neutralize 6 mol of protons.

The equilibria proposed in Scheme 1 involve the formation of mono- and dinuclear species as well as the dissociation of water molecules coordinated to the metal. These species were used to fit the potentiometric titration data with the best standard deviations and the equilibrium constants for the corresponding reactions (first column in Table 4). Thus, these constants were calculated from the experimental data shown in Figure 4, and the logarithms of the calculated equilibrium constants (log *K*) are given in Table 4.

The potentiometric studies of **1** and **2** showed the interesting formation of dinuclear species $[Ln_2H_{-1}L]^{4+}$ and $[Ln_2(OH)H_{-1}L]^{3+}$ as well as the mononuclear species $[LnH_{-1}L]^{+}$, which has a Ln^{III} ion coordinated at the hard side of the H_2L ligand. This finding is in agreement with the ESI-MS data for **1** and **2**.

The potentiometric results also showed the formation of the dinuclear systems 2Ln:2ligand at higher pH values: $[H_{-1}LLn(OH)LnH_{-1}L]^{+}$ and $[H_{-1}LLn(OH)_2LnH_{-1}L]$.

The distribution curves of the species present in solution when complexes **1** and **2** are dissolved are shown and discussed in the next section, together with their reactivity.

Reactivity Studies. In order to investigate the ability of complexes **1** and **2** to promote the hydrolysis of phosphate diester, we employed an activated phosphate diester, BDNPP, as a model substrate for biologically relevant phosphate diesters present in nucleic acids. The rate of hydrolysis was studied as a function of pH as well as catalyst concentration. As evidenced for the complex $[Gd(H_2L)(NO_3)(H_2O)_3](NO_3)_2$,[18] an interesting kinetic behavior was observed from the absorbance versus time profile (Figure S3 in the Supporting Information) for both **1** and **2**, which showed similar catalytic behaviors. We could follow the two saturation curves, referring to the hydrolysis of, first, the diester BDNPP to 2,4-dinitrophenylphosphate (DNPP) and, second, the monoester DNPP to inorganic phosphate. Thus, we can clearly observe the significant difference between the two hydrolysis rates (diester, BDNPP and monoester, DNPP), it being possible to monitor them separately.

The catalytic activity of complexes **1** and **2** toward BDNPP hydrolysis was found to be strongly influenced by the pH of the reaction mixture. The pH dependence of the catalytic activity for BDNPP hydrolysis, that is, the formation of the DNPP intermediate, showed a bell-shaped profile with optimum activity at around pH of 7. The pH:k_{obs} profiles for **1** and **2** can be analyzed in association with the distribution curves of the species formed in solution (Figure 5).

(42) Baes, Jr. C. F.; Mesmer, R. E. *The Hydrolysis of Cations*; John Wiley & Sons: New York, 1976, pp 129−146.

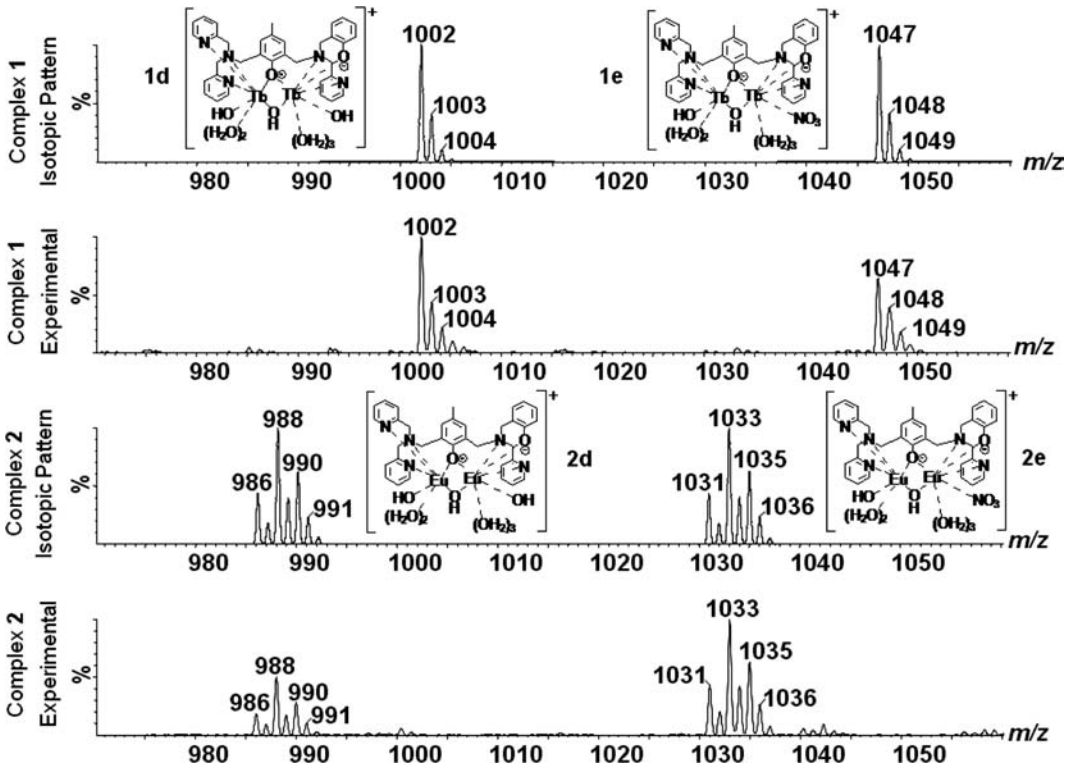

Figure 3. ESI(+)-MS spectra of an acetonitrile/water (75:25) solutions of **1** and **2** in the *m*/*z* range of 980−1050 (experimental), and the isotopic patterns calculated for **1d**, **1e**, **2d**, and **2e**.

Table 4. Equilibrium constants for Formation of Mono- and Dinuclear Species and Dissociation Constants of Water Molecules Coordinated to Ln^{III}

equilibrium		log K^a	
		Tb^{III}	Eu^{III}
$\frac{[HL]}{[L^-][H^+]}$	12.58[b]	–	–
$\frac{[H_2L^+]}{[HL][H^+]}$	6.76[b]	–	–
$\frac{[H_3L^{2+}]}{[H_2L^+][H^+]}$	3.98[b]	–	–
$\frac{[Ln(OH)^{2+}][H^+]}{[Ln^{3+}]}$		−7.9[c]	−7.8[c]
$\frac{[Ln_2H_{-1}L^{4+}][H^+]}{[Ln^{3+}]^2[L^-]}$		7.78	7.76
$\frac{[Ln_2(OH)H_{-1}L^{3+}][H^+]}{[Ln_2H_{-1}L^{4+}]}$		−6.45	−6.64
$\frac{[LnH_{-1}L^+][H^+]}{[Ln^{3+}][L^-]}$		2.57	2.77
$\frac{[H_{-1}LLn(OH)LnH_{-1}L^+][H^+]^3}{[Ln^{3+}]^2[L^-]^2}$		−0.02	0.03
$\frac{[H_{-1}LLn(OH)_2LnH_{-1}L][H^+]}{[H_{-1}LLn(OH)LnH_{-1}L^+]}$		−10.48	−10.12

[a] Log of the equilibrium constants for the equilibria in column 1. [b] Protonation constants for the ligand (L^{-1}), [c] Formation constants for monohydroxo Ln^{3+} complexes at 25 °C with ionic strength of 0.01 mol L^{-1} (KCl).[42]

The results in Figure 5 show that the reactivity of the complexes is significantly higher than that of the free ions, coordination compounds being formed only at pH > 6. The first compound formed is the dinuclear $[Ln_2H_{-1}L]^{4+}$ (B) species, with no dissociated water molecule, which probably leads to its low catalytic activity. However, the dissociation of one bound water molecule in B results in

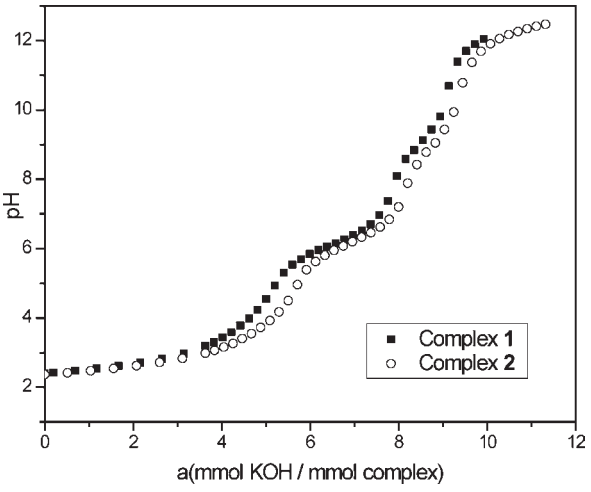

Figure 4. Titration curves for 0.05 mmol of complexes **1** and **2** in an acetonitrile/water solution, μ = 0.1 mol L^{-1} (KCl) at 25 °C; *a* is the number of added KOH equivalents.

the formation of the dinuclear $[Ln_2(OH)H_{-1}L]^{3+}$ (C) species. Table 5 shows the kinetic pK_a values obtained from the standard equation derived from the diprotic model[43] for the fit of the pH versus k_{obs} curve (superimposed dashed line curve in Figure 5), together with the potentiometric pK_a values for the equilibrium: $[Ln_2H_{-1}L]^{4+} = [Ln_2(OH)H_{-1}L]^{3+} + H^+$, with Ln = Tb^{III} or Eu^{III}. Thus, we can observe reasonable agreement between the kinetic and the potentiometric pK_a values, which suggests that the dinuclear $[Ln_2(OH)H_{-1}L]^{3+}$ (C) species, with one hydroxo group, is the most prominent catalyst in the hydrolysis of the diester BDNPP, with maximum formation at pH of 7.

(43) Segel, I. H. *Enzyme kinetics behavior and analysis of rapid equilibrium and steady-state enzyme systems*; Wiley: New York, 1975.

Scheme 1. Proposed Equilibria[a]

1) $2Ln^{3+} + L^{-} \rightleftharpoons [Ln_2H_{-1}L]^{4+} + H^{+}$

2) $[Ln_2H_{-1}L]^{4+} \rightleftharpoons [Ln_2(OH)H_{-1}L]^{3+} + H^{+}$

3) $Ln^{3+} + L^{-} \rightleftharpoons [LnH_{-1}L]^{+} + H^{+}$

4) $2Ln^{3+} + 2L^{-} \rightleftharpoons [H_{-1}LLn(OH)LnH_{-1}L]^{+} + 3H^{+}$

5) $[H_{-1}LLn(OH)LnH_{-1}L]^{+} \rightleftharpoons [H_{-1}LLn(OH)_2LnH_{-1}L] + H^{+}$

[a] $(H_2O)n$ coordinated to Ln^{3+} (Tb or Eu) ions were omitted to facilitate the visualization of these species and the proposed equilibria.

Table 5. Kinetic and Potentiometric pK_a Values for the Equilibrium $[Ln_2H_{-1}L1]^{4+} = [Ln_2(OH)H_{-1}L1]^{3+} + H^+$, with Ln = Tb^{III} or Eu^{III}

$\frac{[Ln_2(OH)H_{-1}L^{3+}][H^+]}{[Ln_2H_{-1}L^{4+}]}$	Ln = Tb^{III}	Ln = Eu^{III}	Ln^{18} = Gd^{III}
kinetic pK_a	5.83	6.04	6.03
potentiometric pK_a	6.45	6.64	6.59

It is interesting to note that the pK_a values obtained for the complexes follow the order: **1** < Gd complex[18] < **2** (Table 5). This is probably a reflection of the decrease in the ionic radius and, consequently, an increase in the electronic density, making the Tb^{III} ion the most acid (compared with Eu^{III} and Gd^{III}), and thus the species $[Tb_2(OH)H_{-1}L]^{3+}$ has the lowest pK_a value.

Figure 5 shows a decrease in reactivity at pH > 7, corresponding to the formation of the $[LnH_{-1}L1]^{+}$ (**D**) species, in which the mononuclear species has the Ln^{III} ion coordinated to the hard side of the ligand (ESI-MS: m/z 702 for Ln = Tb and 696 for Ln = Eu) without dissociated water molecules and, consequently, with no nucleophilic attack of Ln-bound OH^- on the diester bond. At higher pH values, it is possible to observe the formation of dinuclear species of the type 2Ln:2ligand ($[H_{-1}L1Ln(OH)LnH_{-1}L1]^{+}$ (**E**) and $[H_{-1}L1Ln(OH)_2LnH_{-1}L1]$ (**F**)), in which the presence of relatively poor nucleophile groups (μ−OH) and the steric hindrances in excess of substrate in these species is most likely to be responsible for their low catalytic activity.

In the second step of the hydrolysis reaction, the monoester DNPP hydrolyzes to inorganic phosphate, catalyzed by complexes **1** and **2,** also demonstrating the influence of the pH in the reaction. A nonsymmetric bell-shaped pH versus rate profile (Figure S4 in the Supporting Information) was obtained with an optimum pH at around 8.0, which is one pH unit higher than that found in the hydrolysis of the diester BDNPP. This is consistent with the hypothesis that DNPP is bound to the dinuclear catalyst in a bidentate fashion, thus reducing the Lewis acidity of the corresponding metal center.

Complete kinetic studies were performed at the optimum pH value of 7.0, at which it is believed that the dinuclear species $[Ln_2(OH)H_{-1}L]^{3+}$ (Ln = Tb^{III} or Eu^{III}) is the principal species present in solution. The BDNPP hydrolysis rates show a nonlinear dependence on the complex concentrations (**1** and **2**). Considering a system of consecutive reactions,[44] it was possible to deduce the rate law (eq 1 and Figure S5 in the Supporting Information) for the reaction under conditions of excess complex for the hydrolysis of the diester BDNPP:

$$k_{obs} = \frac{k_1 K_1 [C]}{1 + K_1 [C]} \quad (1)$$

where k is the observed rate constant, k_1 is the hydrolysis rate constant, K_1 is the association constant, and $[C]$ is the concentration of complex.

The kinetic parameters for BDNPP hydrolysis were obtained from a nonlinear least-squares fit of k_{obs} versus $[C]$ (Figure S6 in the Supporting Information), giving the constants shown in Table 6. The first-order rate constants of complexes **1** and **2** correspond to an enhancement in the reaction rate of 40 and 100 million times, respectively, in comparison to the spontaneous hydrolysis (1.89×10^{-7} s^{-1}).[20] In addition, these values are about 1000 times higher than the rate constants obtained for the hydrolysis of the same substrate (BDNPP) catalyzed by lanthanide−BTP systems.[45]

On comparing the reactivity of complexes **1**, **2**, and the Gd complex,[18] an increase in the rate (BDNPP hydrolysis) can be observed in the following order: **1** < Gd complex ≅ **2**. Thus, a decrease in the catalytic activity is observed with a reduction in the ionic radius. This means that there is an increase in the electrophilicity of the cation which can lead to a decrease in the basicity of the bound hydroxide anions. Thus, the $[Tb_2(OH)H_{-1}L]^{3+}$ species having the lowest ionic radius (compared with Gd^{III} and Eu^{III}) and, consequently, higher electrophilicity, probably means that the nucleophilic hydroxide group has less basicity, making it less reactive. This correlation has also been found for the catalytic effect of other lanthanide complexes in substitution reactions involving phosphorus.[46]

In the second step of the reaction, the hydrolysis of the monoester DNPP to inorganic phosphate was shown to be independent of the complex concentration for both systems: **1** ($k_2 = 0.6 \times 10^{-2}$ s^{-1}) and **2** ($k_2 = 0.9 \times 10^{-2}$ s^{-1}). Thus, it is suggested that the DNPP hydrolysis occurs through an intramolecular nucleophilic attack of the hydroxo bound to the metal center.

In summary, complexes **1** and **2** as with the Gd complex[18] show one singular catalytic action toward the hydrolysis of the BDNPP diester: one hydrolysis reaction in two stages where the diesterase and monoesterase activities could be observed and monitored separately, with the first stage dependent on and the second independent of the complex concentration.

As our main goal was to obtain an effective catalyst, a hydrolysis reaction with excess of BDNPP (2×10^{-3} mol. L^{-1}) promoted by complexes **1** and **2** (4×10^{-5} mol·L^{-1}) at 445 nm, pH of 7.00, and 25 °C was also monitored. These data revealed that both complexes can be considered as efficient catalysts and are able to hydrolyze around 6 molecules of substrate in 4 h.

The isotopic effect was evaluated in order to establish whether the nucleophilic attack on the phosphorus atom

(44) Wilkins, R. G. *Kinetics and Mechanism of Reactions of Transition Metal Complexes*, 2nd ed.; VCH: Weinheim, Germany, 1991.

(45) Longhinotti, E.; Domingos, J. B.; da Silva, P. L. F.; Szpoganicz, B.; Nome, F. *J. Phys. Org. Chem.* **2005**, *18*, 167–172.

(46) Gomez-Tagle, P.; Yatsimirsky, A. K. *Inorg. Chem.* **2001**, *40*, 3786–3796.

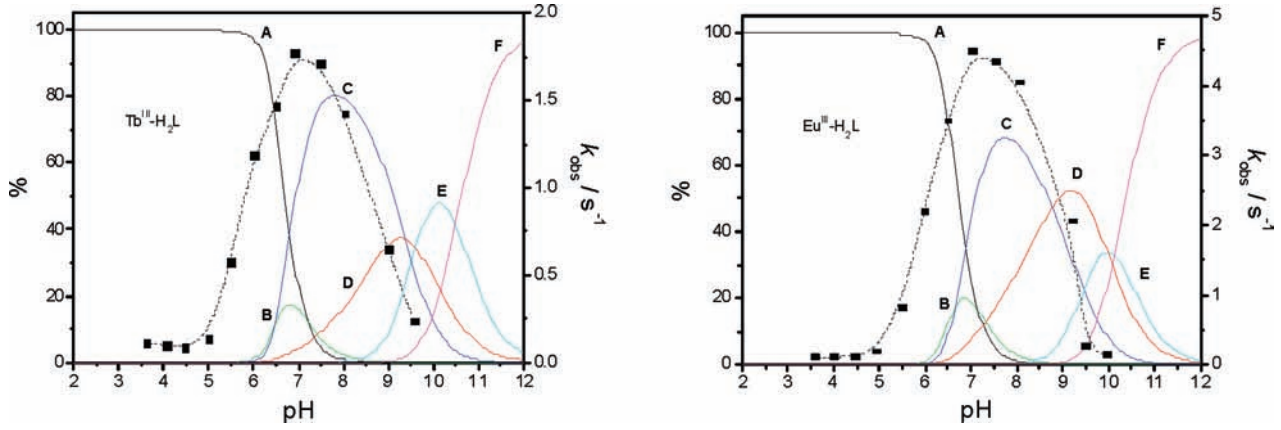

Figure 5. Solid lines representing the species distribution curves of the $Ln^{III}-H_2L$ systems (Ln = Tb and Eu) for dissolution of 0.05 mmol of complexes **1** and **2** in an acetonitrile/water solution, $\mu = 0.1$ mol L^{-1} (KCl) at 25 °C. The dashed line corresponds to a variation in the observed rate constants for the hydrolysis of BDNPP as a function of the pH in an acetonitrile/water solution. Conditions: [**1** or **2**] = 2.0×10^{-3} mol L^{-1} and [BDNPP] = 4×10^{-5} mol L^{-1} at 25 °C. (A) Ln^{III}. (B) $[Ln_2H_{-1}L]^{4+}$. (C) $[Ln_2(OH)H_{-1}L]^{3+}$. (D) $[LnH_{-1}L]^{+}$. (E) $[H_{-1}LLn(OH)LnH_{-1}L]^{+}$. (F) $[H_{-1}LLn(OH)_2LnH_{-1}L]$, with Ln = Tb^{III} or Eu^{III}.

Table 6. Kinetic Parameters Obtained from the First Stage in BDNPP Hydrolysis Catalyzed by Complexes **1**, **2**, and the Isostructural Gd Complex[18] at pH 7, in Acetonitrile/Water (3:1 v/v)[a]

complexes	complex **1**	complex **2**	Gd complex[b]
k_1 (s^{-1})	7	18	17
K_1 (mol^{-1} L)	151	166	158

[a] Conditions: [BDNPP] = 4×10^{-5} mol L^{-1}; [complexes] = 5×10^{-4} to 5×10^{-3} mol L^{-1}; buffer HEPES; $I = 0.1$ mol L^{-1} ($LiClO_4$) at 25 °C. [b] Data from ref 18.

was via the terminal hydroxide ion or a general base catalysis. According to Burstyn and coworkers,[47] when $0.80 < (k_H/k_D) < 1.50$, this is indicative that there is no proton transfer involved in the reaction limiting step, suggesting, thus, an intramolecular nucleophilic attack mechanism. The k_H/k_D ratios obtained for different concentrations of complexes **1** and **2** (Table T1 in the Supporting Information) corroborates the presence of a hydrolysis reaction proceeding through an intramolecular mechanism, in which the phosphorus atom undergoes a nucleophilic attack promoted by the hydroxide ion present in the active species $[Ln_2(OH)H_{-1}L]^{3+}$ (Ln = Tb^{III} or Eu^{III}).

Considering the solid state structures, equilibrium and ESI-MS studies in aqueous solution and the reactivity results reported here for complexes **1** and **2** and those previously reported for the Gd complex,[18] it is reasonable to propose a common mechanism of action for the hydrolysis reaction of the diester BDNPP promoted by these catalysts (Scheme 2). In the first stage, monodentate binding of the BDNPP diester to the metal ion component of the $[Ln_2(OH)H_{-1}L]^{3+}$ species with displacement of a coordinated water molecule (K_1) occurs. This process is followed by a nucleophilic attack on the phosphorus atom by a conveniently oriented terminal Ln-bound hydroxide and a concomitant release of 2,4-dinitrophenolate. The hydrolysis of the intermediate (monoester) to inorganic phosphate is proposed to occur through intramolecular attack of a second Ln-bound OH^- group, probably a μ-OH^- group (poorer nucleophile generated within the intermediate),[48] which explains the monoester hydrolysis being around 1000 times slower than the diester hydrolysis. Alternatively, the monoester may not be adequately oriented for a specific nucleophilic attack of a Ln-bound hydroxide, hindering its hydrolysis.

DNA Interaction. The effects of complex concentration and pH on the nucleic acid cleavage activity were evaluated. Experiments were carried out under identical conditions at pH of 6.1, 6.5, 7.0, and 7.5 with selected complex concentrations (0−160 μM) for **1** and **2,** and the results are shown in Figure 6.

Complexes **1** and **2** effectively promoted the cleavage of supercoiled (form I) DNA to nicked circular (form II) and linear (form III) DNA, the latter suggesting the nonrandom cleavage of double-stranded DNA.

The complexes showed higher activity toward the DNA cleavage at pH 7.0, the same result observed in the hydrolysis of the model substrate BDNPP promoted by **1** and **2**. In the hydrolysis of the model substrate BDNPP, it was proposed that the dinuclear species $[Ln_2(OH)_{H-1}L]^{3+}$ (Ln= Tb^{3+} or Eu^{3+}) is the principal species present in solution at pH of 7 and, consequently, the active species in the catalysis. Thus, kinetic studies were performed at this pH (following the decrease in the percentage of supercoiled form), under conditions of excess complex at 50 °C (Figure S7 and S8 in the Supporting Information). The kinetic parameters obtained for complexes **1** and **2** can be observed in Table 7.

Compared to the estimated uncatalyzed DNA hydrolysis rate,[49] **1** and **2** could accelerate the rate $2.5-2.0 \times 10^7$-fold, respectively. Thus, these complexes have reactivities similar to those of other dinuclear complexes with lanthanide ions that have been shown to cleave DNA through an hydrolytic mechanism.[50]

Complexes **1** and **2** are similarly active in DNA hydrolysis considering k_{cat}, however it seems that complex **1** interacts with the DNA helix more efficiently since its K_M

(47) Deal, K. A.; Hengge, A. C.; Burstyn, J. N. *J. Am. Chem. Soc.* **1996**, *118*, 1713–1718.

(48) Neves, A.; Lanznaster, M.; Bortoluzzi, A. J.; Peralta, R. A.; Casellato, A.; Castellano, E. E.; Herrald, P.; Riley, M. J.; Schenk, G. *J. Am. Chem. Soc.* **2007**, *129*, 7486–7487.

(49) Radzicka, A.; Wolfenden, R. *Science* **1995**, *267*, 90–93.

(50) Branum, M. E.; Tipton, A. K.; Zhu, S.; Que, L., Jr. *J. Am. Chem. Soc.* **2001**, *123*, 1898–1904.

Scheme 2. Mechanism of Action for Complexes in the BDNPP Hydrolysis[a]

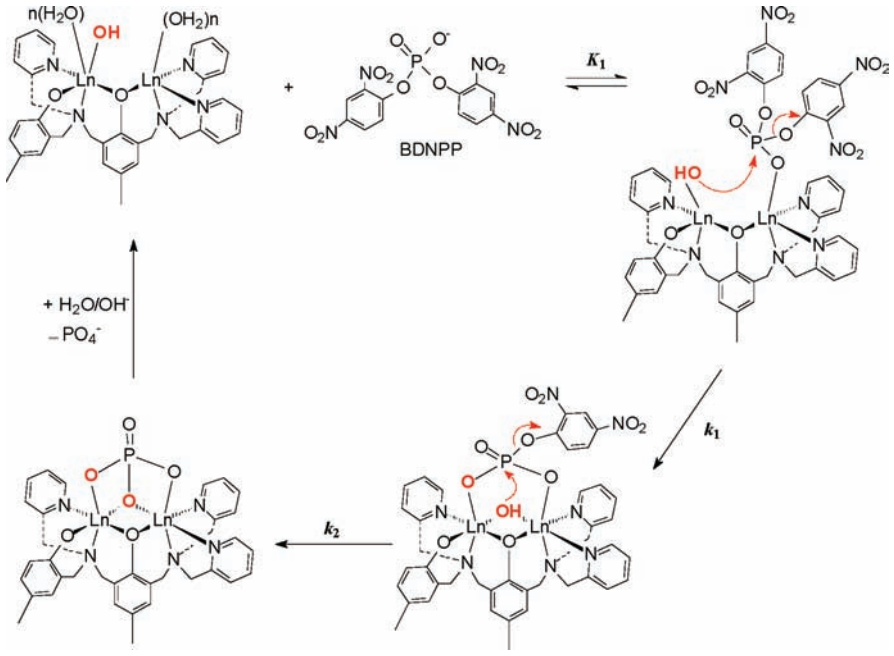

[a] $(H_2O)n$ coordinated to Ln^{3+} (Tb or Eu) ions were omitted to facilitate the visualization of the mechanism proposed.

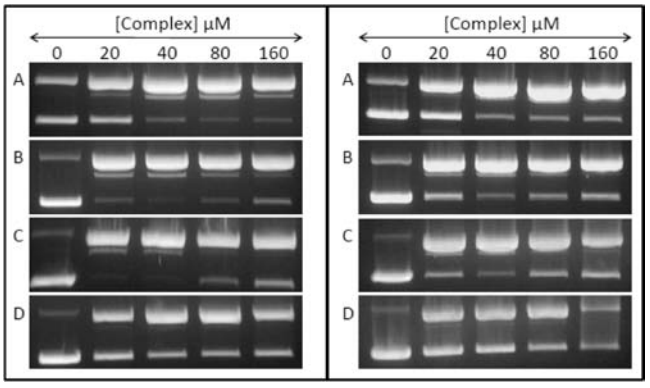

Figure 6. Plasmid DNA cleavage promoted by complexes **1** (left) and **2** (right) at pH of 6.0, 6.5, 7.0, and 7.5 (A, B, C, and D, respectively) at 50 °C and incubation for 6 h. Reactions were performed with pBSK II DNA (40 μM bp) in CH_3CN:H_2O 25:75% and PIPES buffer (25 mM).

Table 7. Kinetic Parameters Obtained in DNA Plasmid Cleavage Catalyzed by Complexes **1**, **2**, and Gd Complex at pH of 7.0 and 50 °C

	K_M (mol L^{-1})	k_{cat} (h^{-1})	$E = k_{cat}/K_M$ (mol^{-1} L h^{-1})	$f = k_{cat}/k_{nc}$
1	5.2×10^{-6}	0.89	1.7×10^5	2.5×10^7
2	3.7×10^{-5}	0.73	2.0×10^4	2.0×10^7
Gd complex	2.5×10^{-5}	0.47	1.8×10^4	1.7×10^7

is lower than that of **2**. Both complexes, **1** and **2**, are more active than the Gd complex previously reported by us.[18]

Complexes **1** and **2** should mediate DNA phosphodiester cleavage through a hydrolytic mechanism because a classical radical scavenger, such as DMSO, was not capable of inhibiting the activity (Figure S9 in the Supporting Information). This is in agreement with the known hydrolytic action of lanthanide ions toward the cleavage of phosphate esters.[51]

(51) Baykal, U.; Akkaya, E. U. *Tetrahedron Lett.* **1998**, *39*, 5861–5864.

Continuing the investigation of the mechanism of action of **1** and **2** in terms of the plasmid DNA cleavage and in order to obtain a greater understanding on the contact surfaces between the catalytic species and the DNA helix, studies were carried out with distamycin, a specific minor groove binder.[52] These studies were performed through an initial incubation of distamycin with plasmid DNA for 30 min at ambient temperature. The corresponding complex was then added, and these systems were incubated for a further 6 h at 50 °C. The results (Figure 7) clearly indicated the inhibition of almost 100% of the complex activity in the presence of distamycin, suggesting that complexes **1** and **2** are regio-specific, interacting with the minor groove of DNA.

Luminescent Studies. The strategy that is usually applied to efficiently photoexcite lanthanide ions, despite their extremely weak absorption, is to use an organic chromophore to absorb the light and then transfer the energy to the lanthanide ion (antenna effect). In this context, complexes **1** and **2**, under UV excitation, displayed green and red luminescence characteristic of trivalent terbium and europium ions, respectively. Luminescence studies with the isostructural Gd complex[18] were also carried out, since it is known that the energy of the first triplet state of a ligand can be determined by measuring the ligand phosphorescence ($T_1 \rightarrow S_0$) in its Gd complexes.[53]

In Figure 8, we can observe the excitation and emission spectra of the solid Gd complex[18] at 25 °C. The band centered at 380 nm in the excitation spectrum corresponds to the first $S_1 \leftarrow S_0$ ligand absorption. Two emission

(52) Tkadlecová, M.; Foltýnová, J.; Valík, M.; Král, V. *Tetrahedron Lett.* **2008**, *49*, 323–326.

(53) de Sá, G. F.; Malta, O. L.; Donegá, C. M.; Simas, A. M.; Longo, R. L.; Santa Cruz, P. A.; Silva, E. F., Jr. *Coord. Chem. Rev.* **2000**, *196*, 165–195.

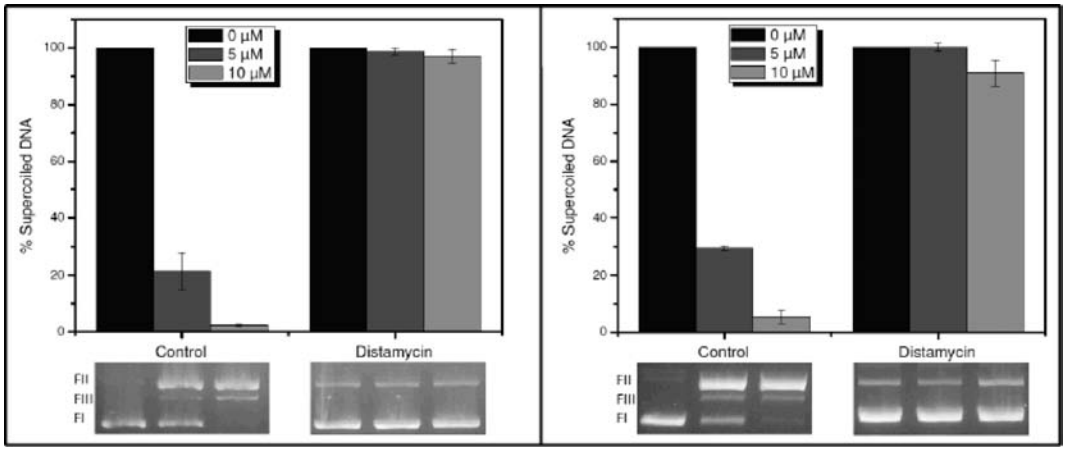

Figure 7. Analysis of plasmid DNA cleavage (pBSK-II, 40 μM bp) catalyzed by complexes **1** (left) and **2** (right), in the absence and presence of distamycin binder (50 μM), after incubation for 6 h at 50 °C at pH of 7.0 (PIPES buffer 25 mM).

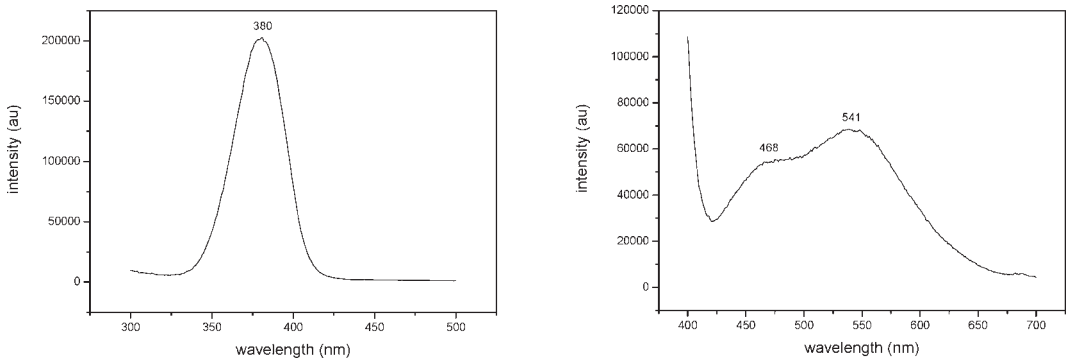

Figure 8. Luminescence spectra of solid $[Gd(NO_3)(H_2L)(H_2O)_3](NO_3)_2$ at 398K: excitation $\lambda_{em} = 541$ nm (left) and emission $\lambda_{ex} = 380$ nm (right).

bands are observed in Figure 8 (see right), the band at 468 nm is attributed to a singlet−singlet transition of the ligand, and the band at 541 nm may be ascribed to the forbidden long-lived triplet−singlet transition. This latter assignment is in agreement with the time-resolved excitation spectrum which shows just one band (Figure S10 in the Supporting Information), indicating that the lowest ligand triplet state is located at 21 050 cm^{-1}.

In general, the main mechanism of the luminescence sensitization of lanthanide ions via the "antenna effect" involves the energy transfer from a ligand-centered triplet state to 4f states of the Ln^{III} ion.[54] Thus, the triplet state of the H_2L ligand at 21 050 cm^{-1} is in a good position to transfer energy to the Tb^{3+} ($^5D_4$) at 20 400 and Eu^{3+} ($^5D_0$) at 17 200 cm^{-1}.

The excitation spectrum of complex **1** (Figure 9) obtained at room temperature shows broad bands centered at around 300 and 345 nm, which are ascribed to ligand absorption and subsequent ligand to Tb^{3+} energy transfer. The emission spectrum (Figure 9, see right) shows characteristic transitions of Tb^{3+} ions, from the $^5D_4$ level to the ^7F_J levels (J = 6 488, 5 545, 4 580, and 3 620 nm).

The excitation spectrum of complex **2** (Figure 10), obtained at liquid nitrogen temperature, shows a prominent band at around 260 nm, which is absent in the excitation spectrum of the Gd complex. This band can be assigned to a ligand-to-metal charge transfer (LMCT) state.[55] The low intensity band centered at around 370 nm can be ascribed to an energy transfer from the ligand triplet state to the Eu^{III} metal ion emitter states (^5D_J). The emission spectrum of complex **2** (Figure 10, see right) presents the characteristic transitions of the Eu^{III} ion $^5D_0 \rightarrow {}^7F_J$ (J = 580, 1590, 2615, 3650, and 4695 nm). It is possible to observe that the $^5D_0 \rightarrow {}^7F_1$ transition has a low intensity compared to those of the $^5D_0 \rightarrow {}^7F_0$ and $^5D_0 \rightarrow {}^7F_2$ transitions and a large number of components, indicating that the Eu^{III} ion is found at the low symmetry site, without an inversion center.[56] This is in agreement with the structure of the mononuclear complex $[Eu(NO_3)(H_2L)(H_2O)_3](NO_3)_2$ resolved by X-ray analysis.

It is interesting to note that complex **1** displays luminescence even at room temperature, and for complex **2**, the corresponding red luminescence is observed only at liquid nitrogen temperature. Since these complexes are isostructural (Tb^{III} and Eu^{III} are found in almost identical coordination environments), the luminescence suppression observed for complex **2** at room temperature may result from the efficient nonradiative deactivation mechanism of the excited states of the Eu^{III} ion via O−H vibrations of the three water molecules coordinated to the metal ion $[Eu(NO_3)(H_2L)(H_2O)_3](NO_3)_2$. Although the H_2L ligand triplet energy level lies above the emitter levels

(54) Bünzli, J.-C. G.; Piguet, C. *Chem. Soc. Rev.* **2005**, *34*, 1048–1077.
(55) Faustino, W. M.; Malta, O. L.; de Sá, G. F. *Chem. Phys. Lett.* **2006**, *429*, 595–599.
(56) Gomes, L. F.; de Oliveira, K. T.; Néri, C. R.; de Sousa Filho, P. C.; Dal Bianco, M. J.; Ramos, A. P.; Zaniquelli, M. E. D.; Serra, O. A. *J. Lumin.* **2008**, *128*, 1339–1347.

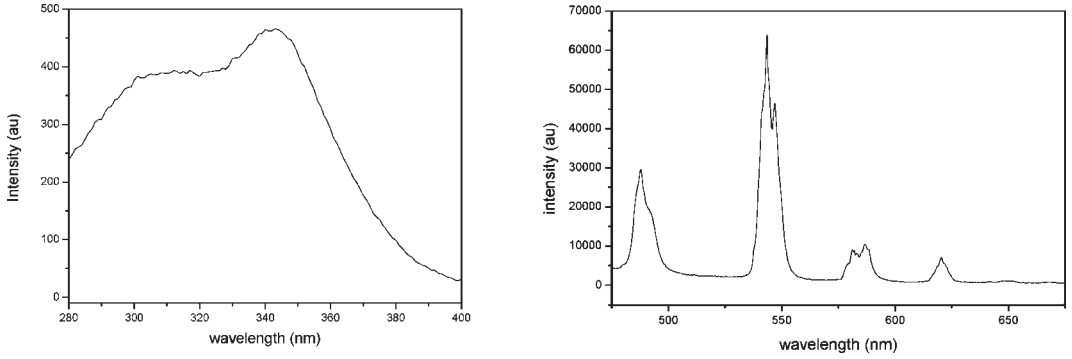

Figure 9. Excitation λ_{em} = 545 nm (left) and emission λ_{ex} = 345 nm (right) spectra of solid $[Tb(NO_3)(H_2L)(H_2O)_3](NO_3)_2$ (**1**), at room temperature.

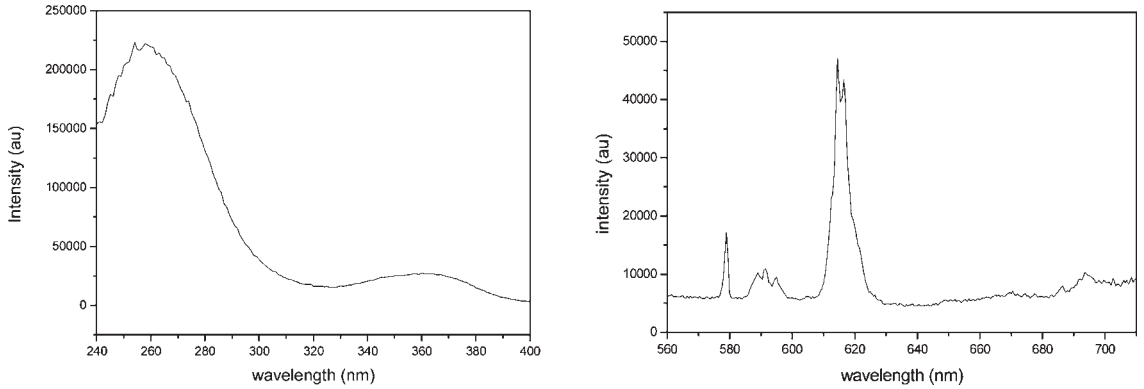

Figure 10. Excitation λ_{em} = 615 nm (left) and emission λ_{ex} = 370 nm (right) spectra of solid $[Eu(NO_3)(H_2L)(H_2O)_3](NO_3)_2$ (**2**), at liquid nitrogen temperature.

of the Eu^{III} (resulting in an efficient sensitization), the observed emission intensity is low due to the high number of vibrational oscillators which contribute to a multiphonon deactivation of the excited states.[57] For the Tb^{III} compound, even though some back transfer ($^5D_4 \rightarrow T_1$ energy transfer) processes can occur with an appreciable intensity, the ligand antenna effect is prominent due to the proximity of the energy levels and lower contribution of vibrational deactivation (Figure S11 in the Supporting Information).

A relevant characteristic of nonradiative luminescence quenching channels (multiphonon decays and LMCT state) is that they are thermally activated,[58] which explains the observation of the luminescence of the Eu^{III} ion (complex **2**) only at liquid nitrogen temperature.

The luminescence lifetimes of complex **1** in aqueous (H_2O/CH_3CN_{dry}) and deuterated water (D_2O/CH_3CN_{dry}) media are long, being 0.58 and 1.00 ms, respectively, allowing the number of inner-sphere coordinated water molecules to be calculated (Horrocks equation)[59] as 3 (uncertainty ±10%). As these experimental media are similar to that utilized in the kinetic studies, where the catalytic dinuclear species is the most prominent species present in the solution, the lifetime values are consistent with three water molecules coordinated to each metal ion.

The lifetime of the $^5D_0$ level in complex **2** is 0.24 ms in solid state at liquid nitrogen temperature. Applying the simplified Barthelemy−Choppin expression,[60] it is estimated that an average of 3.7 water molecules are coordinated to the Eu^{III} ion. Considering the experimental error, this result is consistent with the three coordinated water molecules revealed by X-ray analysis of the complex.

Conclusions

In summary, we have synthesized and structurally characterized two new mononuclear Ln^{III} complexes, with Ln^{III} = Tb (complex **1**) and Eu (complex **2**). As demonstrated in this study, complexes **1** and **2** showed similar catalytic behavior toward the hydrolysis of the 2,4-bis(dinitrophenyl)phosphate (BDNPP) diester, in which the diesterase and monoesterase activities could be observed and monitored separately. These complexes were shown to be highly active in the hydrolysis, with catalytic factors in the order of millions, and data have been collected to suggest that a dinuclear species is the most prominent catalyst under mild conditions. Complexes **1** and **2** were also able to cleave hydrolytically the plasmid DNA at relatively low complex concentrations and under mild conditions of temperature and pH. Furthermore, the interaction of the complexes with DNA were shown to be regio-specific, indicating their potential action as a chemical nuclease. Complexes **1** and **2** displayed luminescent properties, and the study of these properties provided additional information on the active catalytic species.

(57) Bünzli, J.-C. G.; Choppin, G. R. *Lanthanide Probes in Life, Chemical and Earth Sciences*, Elsevier: Amsterdam, The Netherlands, 1989.
(58) Faustino, W. M.; Malta, O. L.; Teotonio, E. E. S.; Brito, H. F.; Simas, A. M.; de Sá, G. F. *J. Phys. Chem. A* **2006**, *110*, 2510–2516.
(59) Horrocks, W. DeW., Jr.; Sudnick, D. R. *J. Am. Chem. Soc.* **1979**, *101* (2), 334–340.
(60) Barthelemy, P. P.; Choppin, G. R. *Inorg. Chem.* **1989**, *28*, 3354–3357.

Acknowledgment. Financial support was received from CNPq, INCT-catálise, FAPESC, and FAPESP. M.A.C. is grateful to CNPq for a postdoc grant (PNPD-151665/2008-7). We thank Dra. Janaína Gomes, Paulo César S. Filho, and Renata F. Martins for assistance during the luminescent experiments.

Supporting Information Available: Crystallographic data of complexes **1** and **2** (atomic coordinates and equivalent isotropic displacement parameter, calculated hydrogen atom parameters, anisotropic thermal parameters, and bond lengths and angles) have been deposited at the Cambridge Crystallographic Data Center (deposition numbers CCDC 766374 and 766375). Copies of this information may be obtained free of charge from: CCDC, 12 Union Road, Cambridge, CB2 1EZ, UK (Fax: +44−1223−336−003; e-mail: deposit@ccdc.cam.ac.uk, or http://www.ccdc.cam.ac.uk. Figures S−S10 show the ESI-MS of complex **1** in solution; ESI-MS of complex **2** in solution; the absorbance vs time profile for BDNPP and DNPP hydrolysis by the complexes; pH dependence for DNPP hydrolysis catalyzed by the complexes; derivation of eq 1; dependence of the reaction rate on the concentration of the complexes in BDNPP hydrolysis; kinetics analysis of DNA cleavage promoted by complex **1**; kinetics analysis of DNA cleavage promoted by complex **2**; the effect of DMSO on the cleavage reaction of DNA catalyzed by the complexes; the time-resolved excitation spectrum of the Gd complex; and the energy level diagram involving the H_2L ligand and the Eu^{III} and Tb^{III} ion. Table T1 shows the k_H/k_D ratios obtained for different concentrations of the complexes. This material is available free of charge via the Internet at http://pubs.acs.org.